Supernova Constraints on Braneworld Dark Energy

Ujjaini Alam[a] and Varun Sahni[a]

[a] *Inter-University Centre for Astronomy and Astrophysics, Post Bag 4, Ganeshkhind, Pune 411 007, India*

Abstract

Braneworld models of dark energy are examined in the light of observations of high redshift type Ia supernovae. Braneworld models admit several novel and even exotic possibilities which include: (i) The effective equation of state of dark energy can be more negative than in LCDM: $w \leq -1$; (ii) A class of braneworld models can encounter a 'quiescent' future singularity at which the energy density and the Hubble parameter remain well behaved, but higher derivatives of the expansion factor ($\ddot{a}$, $\dddot{a}$ etc.) diverge when the future singularity is reached; (iii) The current acceleration of the universe is a *transient feature* in a class of models in which dark energy 'disappears' after a certain time, giving rise to a matter dominated universe in the future. Since horizons are absent in such a space-time, a braneworld model with *transient acceleration* might help reconcile current supernova-based observations of an accelerating universe with the demands of string/M-theory. A maximum likelihood analysis reveals that braneworld models satisfy the stringent demands imposed by high redshift supernovae and a large region in parameter space agrees marginally better with current observations than LCDM. For instance, models with $w < -1$ (> -1) provide better agreement with data than LCDM for $\Omega_m \gtrsim 0.3$ ($\lesssim 0.25$).

I. INTRODUCTION

The idea that the universe may have more than three spatial dimensions first appeared in the works of Kaluza and Klein over 70 years ago. The notion of extra dimensions gradually became popular because of the hope that one might succeed in relating the gauge symmetries of particle physics to the isometries of a compact higher dimensional manifold [1]. All such models, however, assumed that the compactification scale is small ($l \sim l_{\rm Pl} \sim 10^{-33}$ cm) hence unobservable. More recently, the many variants of superstring theory allow for the possibility that at least some of the extra dimensions of nature may be macroscopic. For example, the eleven -dimensional supergravity model of Horava and Witten [2] assumes that ordinary matter fields are confined to a submanifold (brane) which is embedded in a higher dimensional space (bulk). In an important recent development, Randall and Sundrum (RS) examined a simplified variant of this model consisting of a three dimensional brane embedded in a four dimensional anti-de Sitter (AdS) bulk [3]. Their results showed that gravitational excitations are confined close to the brane giving rise to the familiar $1/r^2$ law of gravity, and suggesting that one could identify the brane as our observable universe.

Subsequently the RS ansatz was generalised to incorporate both expanding FRW-type models [4] and anisotropic space-times [5]. Of particular importance to the present study is the observation that simple extensions of the RS scenario can give rise to a universe which is *accelerating*, in agreement with studies of high redshift supernovae [6,7]. It is now well established that high redshift type Ia supernovae appear fainter than expected in a spatially flat matter dominated (Einstein-de Sitter) universe [8,9]. One way of explaining this discrepancy is to postulate that the universe is filled with a smooth component carrying large negative pressure (dark energy). Although several possible candidates for dark energy have been suggested (the cosmological constant, quintessence etc.) none is entirely problem free (see [10,11] for recent reviews).

In this paper we shall focus on a new form of dark energy based on the braneworld model examined in [7,12] (see also [14,15]). Braneworld models of dark energy have interesting new

properties including the fact that, depending upon the form of bulk-brane embedding, the effective equation of state of dark energy can be $w \geq -1$ or $w \leq -1$. In addition, for an appropriate parameter choice, the acceleration of the universe can be a transient phenomenon, thus helping reconcile high-z supernova observations of an accelerating universe with the requirements of string/M-theory.

II. DARK ENERGY FROM BRANEWORLD MODELS

The equations of motion governing the braneworld can be derived from the action [14,15]

$$S = M^3 \left[\int_{\text{bulk}} (R_5 - 2\Lambda_{\text{b}}) - 2 \int_{\text{brane}} K \right] + \int_{\text{brane}} \left(m^2 R_4 - 2\sigma \right) + \int_{\text{brane}} L\left(h_{\alpha\beta}, \phi\right) \, . \qquad (1)$$

Here, R_5 is the scalar curvature of the metric g_{ab} in the five-dimensional bulk, and R_4 is the scalar curvature of the induced metric $h_{\alpha\beta}$ on the brane. The quantity $K = K_{\alpha\beta} h^{\alpha\beta}$ is the trace of the extrinsic curvature $K_{\alpha\beta}$ on the brane defined with respect to its *inner* normal. $L(h_{\alpha\beta}, \phi)$ is the four-dimensional matter field Lagrangian, M and m denote, respectively, the five-dimensional and four-dimensional Planck masses, Λ_{b} is the bulk cosmological constant, and σ is the brane tension. Integrations in (1) are performed with respect to the natural volume elements on the bulk and brane.

The presence of the brane curvature term $m^2 \int_{\text{brane}} R_4$ in (1) introduces an important length scale into the problem $l = 2m^2/M^3$. On short length scales $r \ll l$ (early times) one recovers general relativity, whereas on large length scales $r \gg l$ (late times) brane-specific effects begin to play an important role, leading to the acceleration of the universe at late times [6,16,7]).

The cosmological evolution of the braneworld is described by the Hubble parameter

$$H^2 + \frac{\kappa}{a^2} = \frac{\rho + \sigma}{3m^2} + \underline{\frac{2}{l^2} \left[1 \pm \sqrt{1 + l^2 \left(\frac{\rho + \sigma}{3m^2} - \frac{\Lambda_{\text{b}}}{6} - \frac{C}{a^4} \right)} \right]} \, . \qquad (2)$$

The two signs in (2) correspond to the two separate ways in which the brane can be embedded in the higher dimensional bulk. The underlined term in (2) makes braneworld models

different from standard FRW cosmology. The limiting case of our model $m = 0$ corresponds to the well known FRW generalisation of the RS scenario [4]

$$H^2 + \frac{\kappa}{a^2} = \frac{\Lambda_{\rm b}}{6} + \frac{C}{a^4} + \frac{(\rho+\sigma)^2}{9M^6}\,. \tag{3}$$

In this case, braneworld evolution departs from the standard FRW law at early times when $\rho/\sigma \gg 1$. However, as remarked earlier, braneworld models described by (2) depart from FRW behaviour at *late times*, a property that opens radically new possibilities for the present and future state of our universe.

Braneworld models fall into three main categories [7]:

- 1. **BRANE1** (B1): The Hubble parameter is given by

$$\frac{H^2(z)}{H_0^2} = \Omega_{\rm m}(1+z)^3 + \Omega_\kappa(1+z)^2 + \Omega_\sigma + \underline{2\Omega_l - 2\sqrt{\Omega_l}\,\sqrt{\Omega_{\rm m}(1+z)^3 + \Omega_\sigma + \Omega_l + \Omega_{\Lambda_{\rm b}}}}\,, \tag{4}$$

  where $z = a_0/a(t) - 1$ is the cosmological redshift, while

$$\Omega_{\rm m} = \frac{\rho_0}{3m^2H_0^2}\,, \quad \Omega_\kappa = -\frac{\kappa}{a_0^2H_0^2}\,, \quad \Omega_\sigma = \frac{\sigma}{3m^2H_0^2}\,, \quad \Omega_l = \frac{1}{l^2H_0^2}\,, \quad \Omega_{\Lambda_{\rm b}} = -\frac{\Lambda_{\rm b}}{6H_0^2}\,, \tag{5}$$

  are dimensionless parameters whose values must be determined from observations (the subscript '0' refers to their current value). Ω_σ is determined by the constraint relation

$$\Omega_{\rm m} + \Omega_\kappa + \Omega_\sigma - \underline{2\sqrt{\Omega_l}\,\sqrt{1 - \Omega_\kappa + \Omega_{\Lambda_{\rm b}}}} = 1. \tag{6}$$

- 2. **BRANE2** (B2): The Hubble parameter is given by

$$\frac{H^2(z)}{H_0^2} = \Omega_{\rm m}(1+z)^3 + \Omega_\kappa(1+z)^2 + \Omega_\sigma + \underline{2\Omega_l + 2\sqrt{\Omega_l}\,\sqrt{\Omega_{\rm m}(1+z)^3 + \Omega_\sigma + \Omega_l + \Omega_{\Lambda_{\rm b}}}}\,, \tag{7}$$

  where $\Omega_l < 1 + \Omega_{\Lambda_{\rm b}}$ and Ω_σ is determined from

$$\Omega_{\rm m} + \Omega_\kappa + \Omega_\sigma + \underline{2\sqrt{\Omega_l}\,\sqrt{1 - \Omega_\kappa + \Omega_{\Lambda_{\rm b}}}} = 1. \tag{8}$$

The two models BRANE1 and BRANE2 are complementary and reflect the two distinct ways in which the brane can be embedded in the bulk [7]. Clearly, by setting $\Omega_l = 0$ the underlined terms in (4), (6), (7), (8) vanish and we recover the LCDM model in both cases. The underlined terms in (4) & (7) are caused by braneworld effects and give rise to an important general result, namely

$$H(z)\Big|_{\rm B1} \leq H(z)\Big|_{\rm LCDM}, \qquad H(z)\Big|_{\rm LCDM} \leq H(z)\Big|_{\rm B2} \leq H(z)\Big|_{\rm SCDM}, \tag{9}$$

ie the universe expands at a faster (slower) rate than LCDM in BRANE2 (BRANE1). Since most cosmological observables involve $H(z)$ either directly or indirectly, braneworld models can exhibit properties which can be quite distinct from those of either LCDM or SCDM.

- 3. **Disappearing dark energy** (DDE): The Hubble parameter is given by (7), and the cosmological parameters $\Omega_{\rm m}, \Omega_\sigma, \Omega_l, \Omega_{\Lambda_{\rm b}}$ are constrained to satisfy the following relations [7]:

$$\Omega_l \leq \Omega_{\Lambda_{\rm b}} \Rightarrow \Omega_{\Lambda_{\rm b}} \geq \frac{(1-\Omega_{\rm m})^2}{4\Omega_{\rm m}}\,, \tag{10}$$

$$\Omega_{\rm m} + 2\sqrt{\Omega_l}\left(\sqrt{1+\Omega_{\Lambda_{\rm b}}} - \sqrt{\Omega_{\Lambda_{\rm b}}}\right) = 1, \tag{11}$$

$$\Omega_\sigma = -2\sqrt{\Omega_l \Omega_{\Lambda_{\rm b}}}. \tag{12}$$

(We make the assumption that the universe is spatially flat, so that $\Omega_\kappa = 0$.)

From (4) & (7) it is easy to see that all braneworld models approach the standard matter dominated universe at early times [with a small correction term $\sim (1+z)^{3/2}$]. At late times the behaviour of the braneworld can differ from both LCDM and SCDM. This feature makes braneworld models testable and allows the braneworld scenario to provide a new explanation for the observational discovery of dark energy.

The braneworld models described above provide a common platform for understanding the properties of dark energy. For instance the expression for the Hubble parameter in these models (4) & (7) allows us to explicitly determine key cosmological quantities including:

- The luminosity distance $d_L(z)$:

$$\frac{d_L(z)}{1+z} = c\int_0^z \frac{dz'}{H(z')}\,, \tag{13}$$

- the angular-size distance

$$d_A(z) = \frac{c}{1+z}\int_0^z \frac{dz'}{H(z')}\,, \tag{14}$$

- the deceleration parameter:

$$q(z) = \frac{H'(z)}{H(z)}(1+z) - 1\,, \tag{15}$$

- the effective equation of state of dark energy:

$$w(z) = \frac{2q(z)-1}{3\left[1-\Omega_{\rm m}(z)\right]}\,, \tag{16}$$

- the age of the universe:

$$t(z) = \int_z^\infty \frac{dz'}{(1+z')H(z')}\,, \tag{17}$$

- the 'statefinder pair' [17]:

$$\begin{aligned} r &= \frac{\dddot{a}}{aH^3} \equiv 1 + \left[\frac{H''}{H} + \left(\frac{H'}{H}\right)^2\right](1+z)^2 - 2\frac{H'}{H}(1+z), \\ s &= \frac{r-1}{3(q-1/2)}, \end{aligned} \tag{18}$$

- the product $d_A(z)H(z)$, which is used in the Alcock-Paczynski anisotropy test [18],

- the product $d_A^2(z)H^{-1}(z)$, which plays a key role in the volume-redshift test [19].

While providing a common basis for the existence of dark energy, braneworld models B1, B2, DDE, have important properties and attributes which serve to distinguish these models both from each other, and from alternate models of dark energy such as LCDM & quintessence. For instance, the luminosity distance in BRANE1 *can be larger* than the luminosity distance in LCDM: $d_L|_{B1} \geq d_L|_{LCDM}$. This follows from (9) and leads to an important result. Namely, using (16) we find the current value of the effective equation of state of dark energy:

$$w_0 = \frac{2q_0 - 1}{3\,(1 - \Omega_{\rm m})} = -1 - \frac{\Omega_{\rm m}}{1 - \Omega_{\rm m}} \sqrt{\frac{\Omega_l}{\Omega_{\rm m} + \Omega_\sigma + \Omega_l + \Omega_{\Lambda_{\rm b}}}}\,, \tag{19}$$

from where we see that $w_0 \leq -1$. BRANE1 therefore has the remarkable property that the effective equation of state of dark energy can be more negative than that associated with a cosmological constant ($w = -1$). This feature distinguishes B1 models from LCDM as well as from scalar field based quintessence models.

BRANE2 has the opposite property, namely $d_L|_{SCDM} < d_L|_{B2} \leq d_L|_{LCDM}$, which translates into

$$\begin{aligned} &-1 \leq w_0 < 0, \\ &\text{where } \; w_0 = -1 + \frac{\Omega_{\rm m}}{1 - \Omega_{\rm m}} \sqrt{\frac{\Omega_l}{\Omega_{\rm m} + \Omega_\sigma + \Omega_l + \Omega_{\Lambda_{\rm b}}}}\,. \end{aligned} \tag{20}$$

We therefore see that B1 & B2 are complementary models and that the effective equation of state in B1 (B2) is *softer* (stiffer) than the $w = -1$ typical of LCDM. Furthermore in both B2 & DDE, the current acceleration of the universe – like earlier matter and radiation dominated epochs – can be a *transient feature*. In the case of DDE, the current accelerating phase will be replaced by a matter dominated epoch during which $w \simeq 0$ [7]. In Fig. 1 we show the behaviour of the deceleration parameter for this class of models. It is seen that braneworld dark energy disappears in the future and the universe becomes matter dominated as $z \to -1$. It is easy to show that the present value of the effective equation of state of dark energy in DDE is given by

$$w_0 = -\frac{1}{2} \frac{\sqrt{1 + \Omega_{\Lambda_b}} - \sqrt{\Omega_{\Lambda_b}}}{\sqrt{1 + \Omega_{\Lambda_b}} - \sqrt{\Omega_l}}. \tag{21}$$

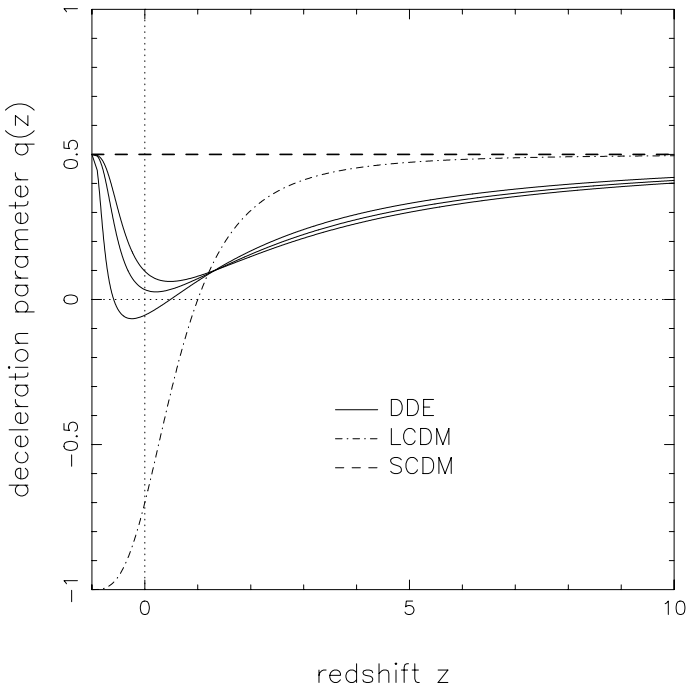

FIG. 1. The behaviour of the deceleration parameter with redshift for DDE. Solid curves from top to bottom are DDE models with $\Omega_m = 0.2$, and $\Omega_{\Lambda_b} = 1.0, 1.5, 2.0$ respectively. The dashed line is SCDM with $\Omega_m = 1$, the dot-dashed curve is LCDM with $\Omega_m = 0.2$. The vertical dotted line marks the present epoch at $z = 0$, and the horizontal dotted line marks a $q = 0$ Milne universe. In the DDE models, the universe ceases to accelerate and becomes matter-dominated in the future, unlike the LCDM model which remains dark energy dominated at all future times.

Since $\Omega_l \leq \Omega_{\Lambda_b}$ we find that $w_0 \geq -0.5$. Model B2 permits more exotic possibilities. In a subclass of models acceleration gives way to an epoch during which the universe decelerates at an increasingly rapid rate [12]. The expansion of the universe culminates in a 'quiescent singularity' which is distinguished from conventional general relativistic singularities by the fact that the energy density and Hubble parameter *remain finite*, while higher derivatives of the scale factor ($\ddot{a}$, $\dddot{a}$ etc.) diverge, when the 'future singularity' is reached (Fig. 2). (The future singularity, measured from the present epoch, is reached in a few billion years for most B2 type braneworld models [12].)

Since neither B2 nor DDE possess an event horizon both can successfully reconcile the demands of string/M-theory with a universe which is currently accelerating [13].

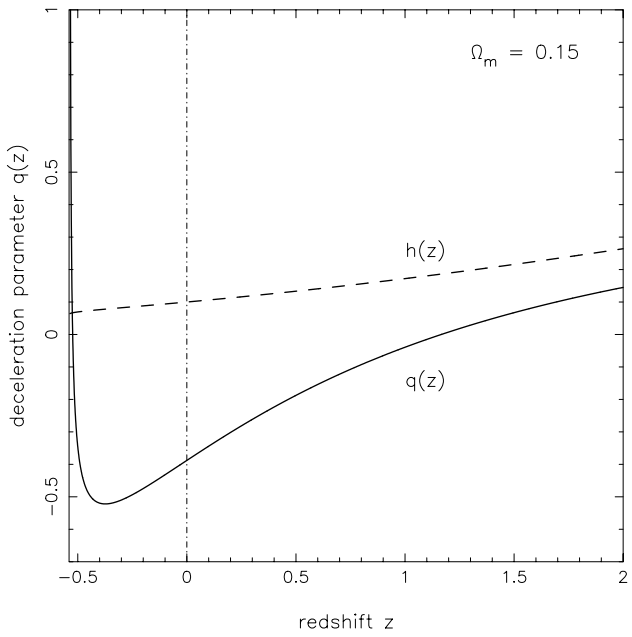

FIG. 2. The BRANE2 universe can encounter a singularity lying in the *future* as demonstrated in this figure. The deceleration parameter becomes infinite as the singularity is approached while the Hubble parameter (and the density, pressure) remain finite. The vertical dot-dashed line corresponds to the present epoch $z = 0$ while the dashed line represents the dimensionless Hubble parameter. The solid line shows the deceleration parameter $q(z)$. The model parameters are $\Omega_m = 0.15,\ \Omega_l = 0.4$. Although permitted by supernovae observations this particular model appears to be disfavored by clustering bounds on Ω_m (see Fig. 6).

III. METHODOLOGY AND RESULTS

We constrain the parameter space of braneworld cosmology by ensuring that our cosmological models provide a good fit to Type Ia supernova data. For this purpose we use the 54 SNe Ia from the primary 'fit C' of the Supernova Cosmology Project, which includes 16 low redshift Calan-Tololo SNe [9]. Fit C is a subsample of a total of 60 SNe of which six are excluded as outliers: two low redshift SNe due to suspected reddening and four high redshift SNe of which two are excluded due to atypical light curves and two because of reddening. The measured quantity in this data, the bolometric magnitude m_B, is related to the luminosity distance and therefore the cosmological parameters by the following equation

$$m_B = \mathcal{M} + 5\,\log_{10} D_L(z; \Omega_m, \Omega_l, \Omega_{\Lambda_b})\ , \tag{22}$$

where $D_L = H_0 d_L$ is the Hubble-parameter-free luminosity distance and $\mathcal{M} = M_B + 25 - 5\,\log_{10} H_0$ is the Hubble-parameter-free absolute magnitude. We shall assume that the SNe measurements come with uncorrelated Gaussian errors in which case the likelihood function is given by the chi-squared distribution with $N - n$ degrees of freedom $\mathcal{L} \propto \exp\left(-\chi^2/2\right)$. (In our case $N = 54$, and $n = 4$: B1 and B2 estimate four parameters each, and DDE estimates three parameters with one constraint, Eq (10) lowering the degrees of freedom)

The χ^2-statistic is defined as

$$\chi^2 = \sum_{i=1}^{54} \left(\frac{m_i^{\rm eff} - m(z_i)}{\sigma_{m_i}} \right)^2\ , \tag{23}$$

where $m_i^{\rm eff}$ is the effective B-band magnitude of the i-th supernova obtained after correcting the observed magnitude at redshift z for the supernova width-luminosity relation, σ_{m_i} is the error in magnitude at redshift z, and $m(z_i)$ is the apparent magnitude of the i-th supernova in the braneworld model.

For BRANE1 and BRANE2, the parameters to be estimated are $\mathcal{M}$, Ω_m, Ω_l, Ω_{Λ_b} (Ω_σ is calculated from Eqs (6) and (8) respectively for B1 & B2). For our purposes the quantity $\mathcal{M}$ is a statistical nuisance parameter, and we marginalise over it assuming no prior

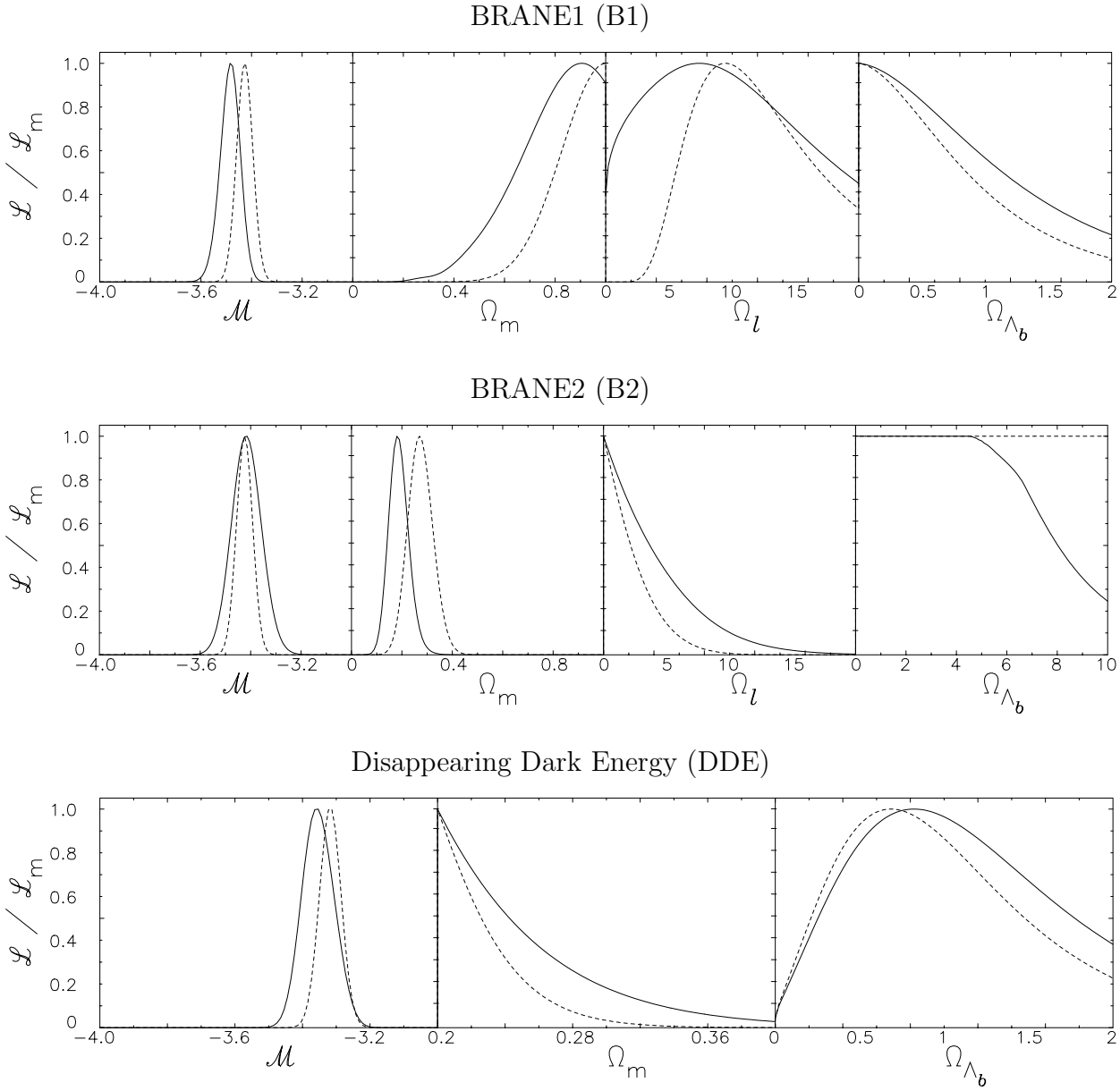

FIG. 3. The likelihood function is shown as a function of each of the parameters Ω_m, Ω_l, Ω_{Λ_b} and $\mathcal{M}$ after the remaining parameters have been marginalised. The top, middle and bottom panels show the likelihood curves for B1, B2, and DDE. The solid lines correspond to the value of the likelihood function for a given parameter after it has been marginalised over all other parameters, while the dashed lines show the likelihood function evaluated by fixing the other parameters at their maximum likelihood value. In all three cases the likelihood function is normalised with the maximum likelihood value set to unity.

knowledge to get the three-dimensional probability distribution in the $(\Omega_m, \Omega_l, \Omega_{\Lambda_b})$ space: $P(\Omega_m, \Omega_l, \Omega_{\Lambda_b}) = \int P(\Omega_m, \Omega_l, \Omega_{\Lambda_b}, \mathcal{M}) d\mathcal{M}$. We perform maximum likelihood analysis on the system with the priors $0 \leq \Omega_m \leq 1,\ \Omega_l \geq 0,\ \Omega_{\Lambda_b} \geq 0$. For B2, we use the added constraint $\Omega_l \leq 1 + \Omega_{\Lambda_b}$. For DDE, the parameters to be estimated are $\mathcal{M}$, $\Omega_m,\ \Omega_{\Lambda_b}$. (The remaining two parameters Ω_l and Ω_σ are related to $\Omega_m,\ \Omega_{\Lambda_b}$ through Eqs (11) and (12) respectively). For this model we use the prior $0 \leq \Omega_m \leq 1$ and the constraint Eq (10) (see [7] Appendix). For B1 & B2 the constraint relations (6), (8) combined with $\Omega_\kappa = 0$, set the lower bound $\Omega_{\Lambda_b} \geq -1$. However since $\Omega_{\Lambda_b} \geq 0$ is a more physically appealing model (it includes anti-de Sitter space (AdS) bulk geometry), we choose this as a prior for further analysis. Results for $-1 \leq \Omega_{\Lambda_b} < 0$ will be presented elsewhere.

In Fig. 3 we show the likelihood curve as a function of $\Omega_m,\ \Omega_l,\ \Omega_{\Lambda_b}$ and $\mathcal{M}$ for the braneworld models B1, B2, and DDE. We see that for all three cases the likelihood is a sharply peaked function of $\mathcal{M}$, which is non-zero over a very limited range. Therefore it seems reasonable to marginalise over $\mathcal{M}$ in this range. Surprisingly, the likelihood function for BRANE1 peaks at $\Omega_{\Lambda_b} = 0$, which is its best-fit value. Thus the BRANE1 universe appears to prefer a *vanishing cosmological constant* in the bulk. The BRANE2 universe shows very different behaviour. In this case the likelihood function is flat and therefore insensitive to the value of Ω_{Λ_b} over the wide range $0 \leq \Omega_{\Lambda_b} \lesssim 5$. Beyond $\Omega_{\Lambda_b} \sim 5$ the likelihood function drops steeply. In Figs 4 and 6 we have shown maximum likelihood contours for B1 and B2 obtained by (a) marginalising over Ω_{Λ_b}, and (b) setting $\Omega_{\Lambda_b} = 0$. The close similarity between these two figures suggests that the likelihood contours marginalised over Ω_{Λ_b} do not change the results appreciably, either for B1 or for B2.

In Fig. 4 we show confidence levels in the $\Omega_m - \Omega_l$ plane for BRANE1. We find that the BRANE1 model can be definitely excluded only if the matter density is small $\Omega_m \lesssim 0.2$. For $\Omega_m \gtrsim 0.3$ the BRANE1 model agrees well with supernovae data, with the agreement extending to larger values of Ω_l as Ω_m increases. Clearly in order to be able to restrict the braneworld parameters further one needs additional information about the dark matter

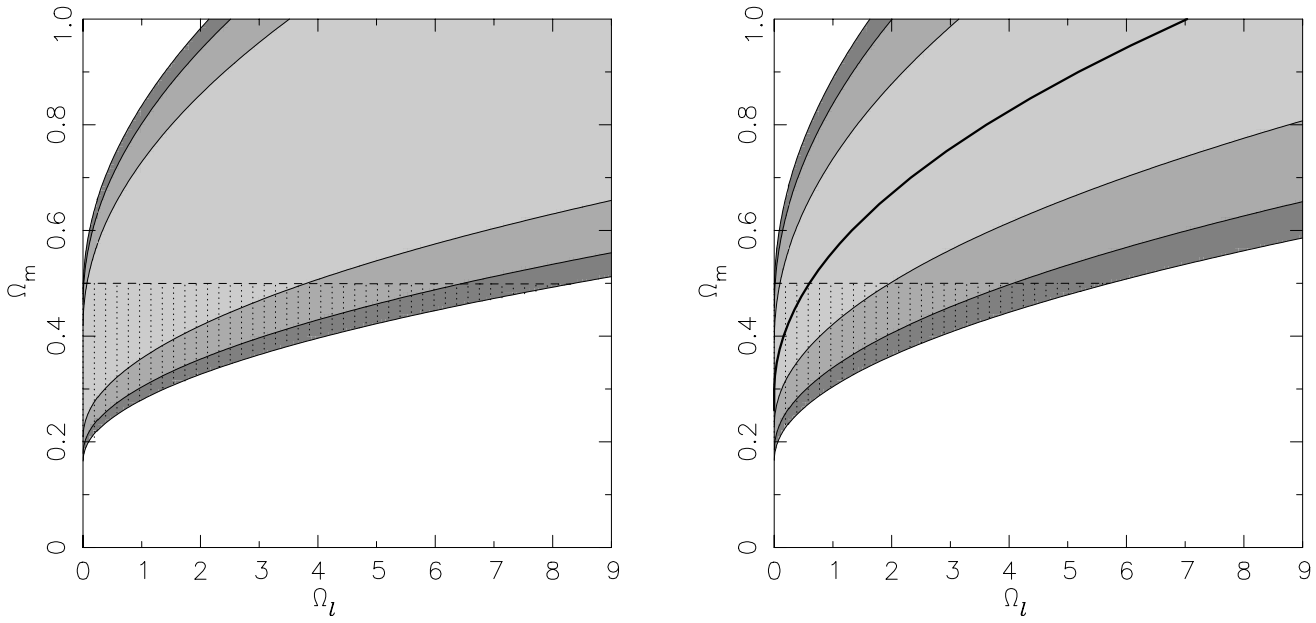

(a) **(b)**

FIG. 4. Confidence levels at 68.3% (light grey inner contour) 95.4% (medium grey contour) and 99.73% (dark grey outer contour) are shown in the Ω_l-Ω_m plane for BRANE1. Panel (a) represents confidence levels in the Ω_l-Ω_m plane when marginalised over Ω_{Λ_b} and $\mathcal{M}$, while panel (b) shows the confidence levels marginalised over $\mathcal{M}$, with $\Omega_{\Lambda_b} = 0$, the best-fit value. We see that taking the best-fit value of $\Omega_{\Lambda_b} = 0$ instead of marginalising over it does not change the results appreciably. The dotted region represents the intersection of the 3σ confidence level with the observational constraint $0.2 \leq \Omega_m \leq 0.5$. The thick solid line in (b) represents the most likely value of Ω_l if the value of Ω_m is known exactly. We see that the BRANE1 model is in good agreement with SNe observations if the value of Ω_m is moderately high: $\Omega_m \gtrsim 0.3$. (It should be noted that the value of the five dimensional Planck mass corresponding to $\Omega_l \sim 1$ is $M \sim 100$ MeV.)

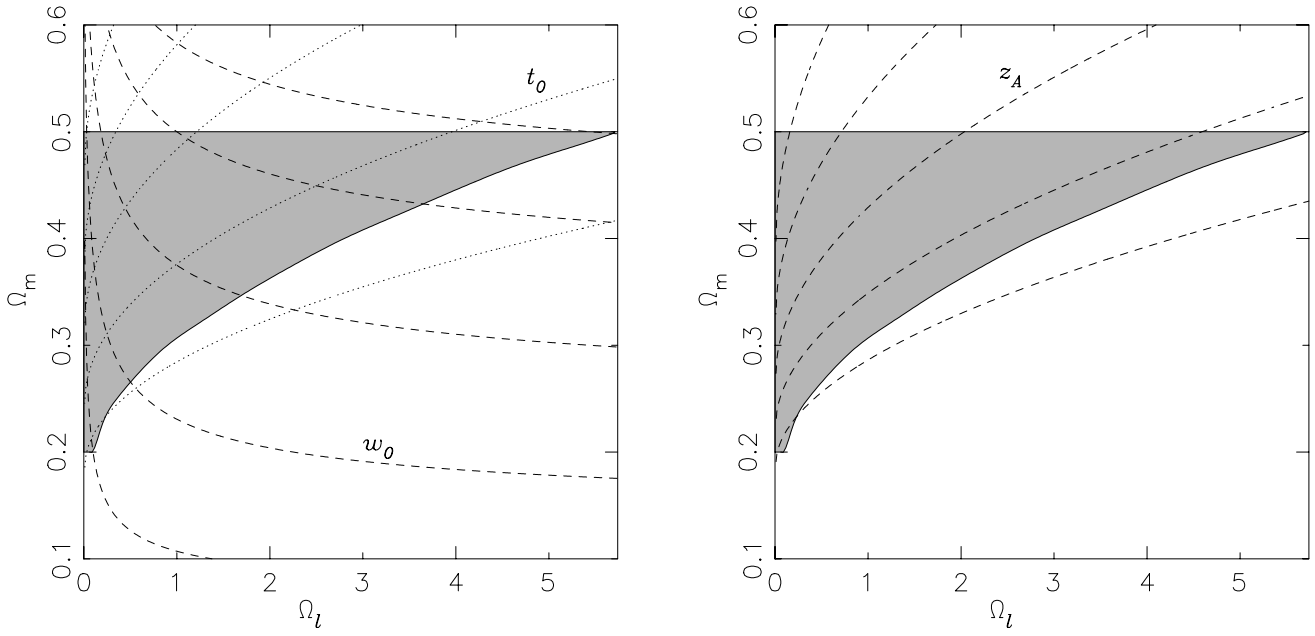

(a) **(b)**

FIG. 5. The shaded region represents the intersection of the 3σ confidence region in the $\Omega_m - \Omega_l$ plane for B1 with the observational constraint $0.2 \leq \Omega_m \leq 0.5$ ($\Omega_{\Lambda_b} = 0$ is assumed). In panel (a) we show the values of different cosmological quantities determined at the present epoch. The dashed lines correspond to the current effective equation of state of braneworld dark energy for BRANE1 models: $w_0 = -1.70,\ -1.50,\ -1.30,\ -1.15,$ and -1.05 (top to bottom). The dotted lines correspond to the current age of the BRANE1 universe: $H_0 t_0 = 0.85,\ 0.90,\ 0.95,\ 1.02,$ and 1.10 (top to bottom). This corresponds to $t_0(\text{Gyrs}) = 11.8,\ 12.6,\ 13.3,\ 14.3$ and 15.4 if $H_0 = 70$ km/sec/Mpc. In panel (b) the dashed lines correspond to the epoch, z_A, at which the braneworld universe (B1) begins to accelerate: $z_A = 0.45,\ 0.60,\ 0.75,\ 0.90,$ and 1.05 (top to bottom).

density not included in the supernova observations. Currently there is no firm consensus on the value of Ω_m. While recent studies of galaxy clustering indicate $\Omega_m \sim 0.3$ [20], larger values of Ω_m may be favoured by observations of clusters of galaxies [21,22]. In this paper we shall assume the weak clustering bound $0.2 \lesssim \Omega_m \lesssim 0.5$ and study the braneworld models in greater detail in this region. In figure 4 the intersection of the '3σ' SNe bound and the bound on Ω_m is shown as a dotted region. Interestingly a large region in BRANE1 parameter space is seen to satisfy both the supernova constraints as well as the clustering bounds on Ω_m.

Fig. 5 highlights the $\Omega_m - \Omega_l$ region permitted both by the SNe bound on BRANE1 and by the clustering bound $0.2 \lesssim \Omega_m \lesssim 0.5$ for the best-fit value $\Omega_{\Lambda_b} = 0$. The lines running through the region depict, respectively, (i) different values of the current effective equation of state, w_0, of dark energy, (ii) the age of the universe, t_0, (iii) the *acceleration epoch*, z_A, defined as the redshift at which the universe began to accelerate. We find that the age of the universe is constrained to lie in the range $0.85 \lesssim t_0 H_0 \lesssim 1.10$, while the effective equation of state is $-1.70 \lesssim w_0 \lesssim -1$ (One should note that $w_0 \leq -1$ in the BRANE1 model) . From the figure we find that the acceleration of the BRANE1 universe is a fairly recent phenomenon, which commenced at $0.45 \lesssim z_A \lesssim 1.05$.

Fig. 6 shows the confidence levels in the $\Omega_m - \Omega_l$ plane for the BRANE2 model. Again the intersection of the '3σ' SNe bound with the bound $0.2 \leq \Omega_m \leq 0.5$ is shown as the dotted region. In contrast to BRANE1 *lower values of* Ω_m *agree better with observations* for BRANE2. The region to the right of the dashed line in the figure corresponds to the class of braneworld models having future singularities. It is interesting to note that such models are in good agreement with SNe data for low values of Ω_m, but are ruled out (at 3σ) if $\Omega_m \gtrsim 0.25$.

Fig. 7 shows lines of constant w_0, t_0, and z_A within the allowed region for BRANE2. Our results show that, the age of the universe, its effective equation of state, and the commencement of acceleration epoch, are constrained to lie within the following intervals: $0.88 \lesssim H_0 t_0 \lesssim 1.07$, $-1 \lesssim w_0 \lesssim -0.6$, and $0.4 \lesssim z_A \lesssim 1$. (One should note that $w_0 \leq -1$

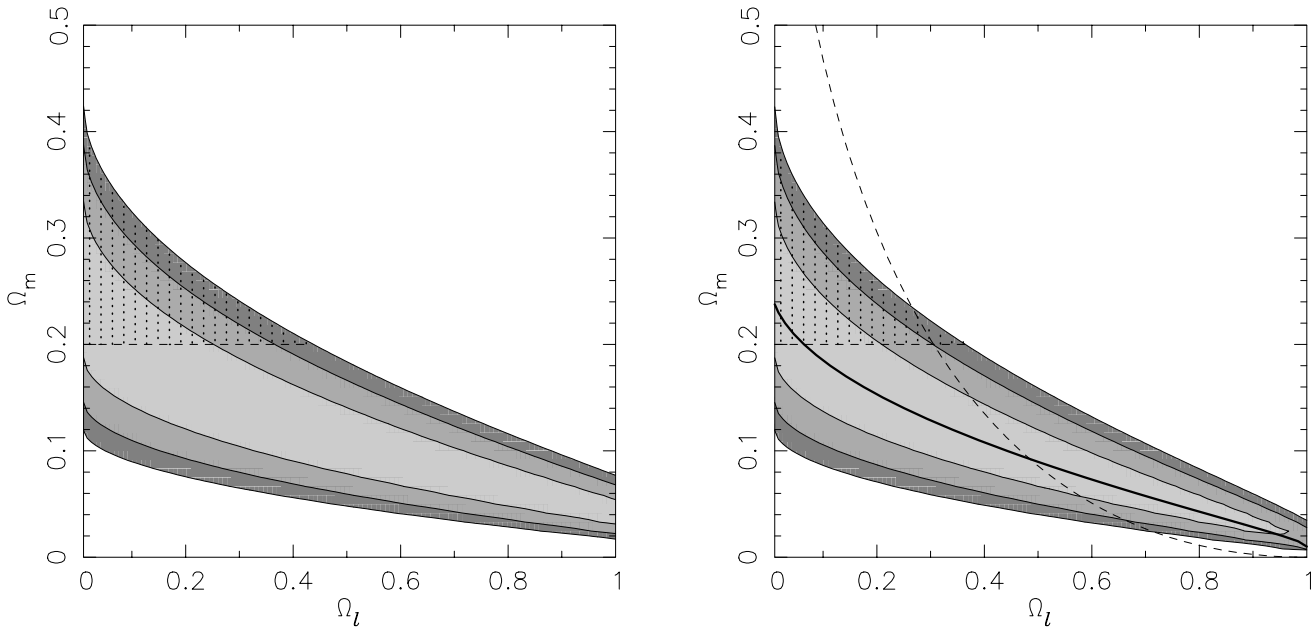

FIG. 6. Confidence levels at 68.3% (light grey inner contour) 95.4% (medium grey contour) and 99.73% (dark grey outer contour) are shown in the Ω_l-Ω_m plane for the BRANE2 model. The figure (a) represents confidence levels in the Ω_l-Ω_m plane when marginalised over Ω_{Λ_b} and $\mathcal{M}$, while the figure (b) shows the confidence levels marginalised over $\mathcal{M}$, with $\Omega_{\Lambda_b} = 0$. We see that fixing the value of Ω_{Λ_b} to zero instead of marginalising over it has negligible effect on the results. The dotted region represents the intersection of the 3σ confidence level with the observational constraint $0.2 \leq \Omega_m \leq 0.5$. The thick solid line in (b) represents the most likely value of Ω_l if the value of Ω_m is known exactly. The region to the right of the dotted line in (b) represents B2 universes which will encounter future 'quiescent' singularities. We see that the BRANE2 model is in good agreement with SNe observations for lower values of $\Omega_m \lesssim 0.30$.

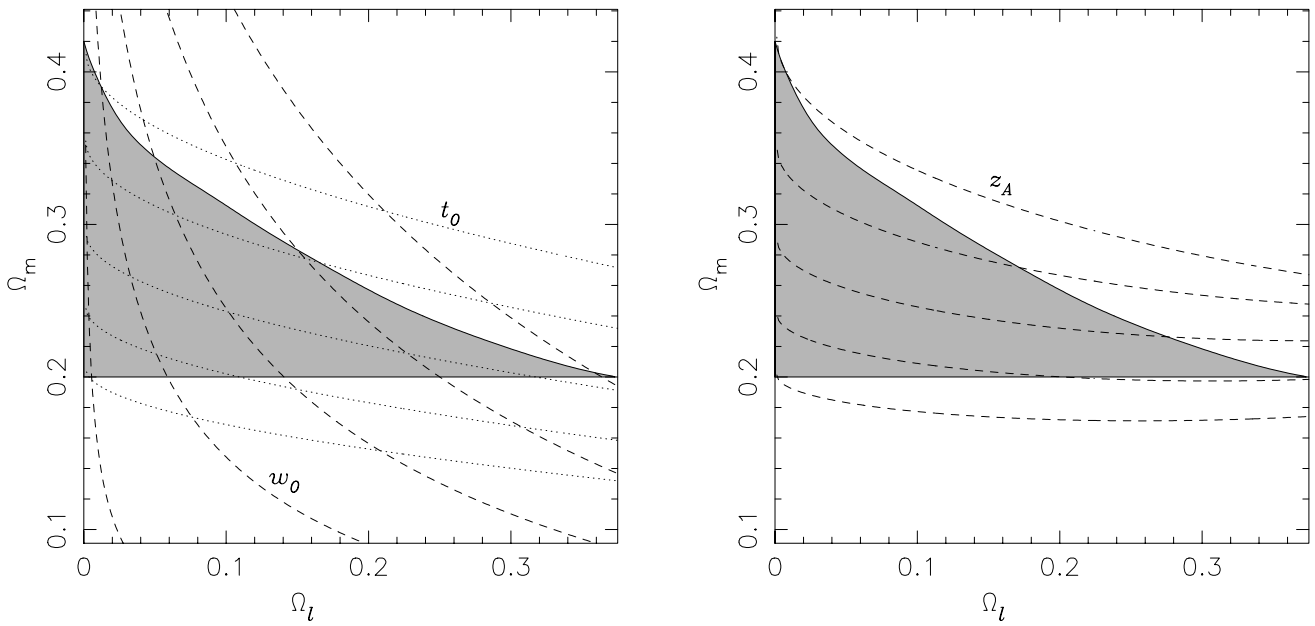

(a) **(b)**

FIG. 7. The shaded region represents the intersection of the 3σ confidence level of BRANE2 for $\Omega_{\Lambda_b} = 0$ with the observational constraint $0.2 \leq \Omega_m \leq 0.5$. In (a) we show the values of different cosmological quantities determined at the present epoch. The dashed lines correspond to the current effective equation of state of braneworld dark energy for BRANE2 models: $w_0 = -0.62,\ -0.75,\ -0.85,\ -0.92$ and -0.98 (top to bottom). The dotted lines correspond to the current age of the BRANE2 universe: $H_0 t_0 = 0.88,\ 0.92,\ 0.97,\ 1.02,$ and 1.07 from (top to bottom). This corresponds to t_0(Gyrs) $= 12.3,\ 12.9,\ 13.5,\ 14.3,$ and 14.9 if $H_0 = 70$ km/sec/Mpc.. In (b) the dashed lines correspond to $z_A = 0.40,\ 0.55,\ 0.70,\ 0.85,$ and 1.00 (top to bottom), where z_A is the epoch at which the braneworld universe (B2) begins to accelerate.

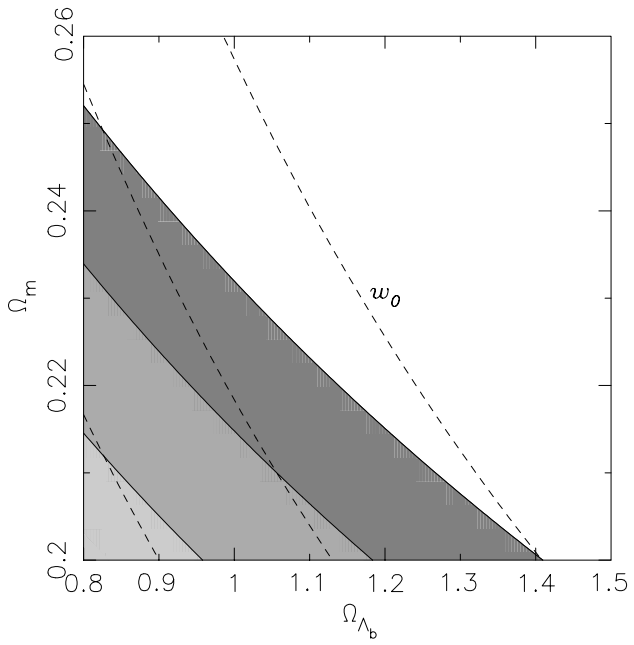

FIG. 8. Confidence levels at 68.3% (light grey inner contour) 95.4% (medium grey contour) and 99.73% (dark grey outer contour) in the Ω_{Λ_b}-Ω_m plane for the 'Disappearing Dark Energy' (DDE) model . The dashed lines show the current effective equation of state: $w_0 = -0.48, -0.44, -0.4$ (left to right).

in the BRANE2 model).

Next we come to the third braneworld model, namely 'Disappearing Dark Energy' (DDE) for which the confidence levels in the $\Omega_m - \Omega_{\Lambda_b}$ plane are shown in figure 8. This case is different from the others in that the best fit value of Ω_m tends to zero for this model. This behaviour is easily understood in view of the fact that the effective equation of state in this model (21) is always constrained to be $\gtrsim -0.5$ and therefore cannot be very negative. Since the luminosity distance increases as Ω_m decreases, a sufficiently large value of the luminosity distance (which agrees well with SNe observations) can only be achieved at the expense of having a small value of Ω_m in our braneworld model. Our results, shown in figure 8, are for the DDE model constrained by the prior $\Omega_m \geq 0.2$. The best fit DDE model ($\Omega_m = 0.2,\ \Omega_{\Lambda_b} = 0.8$) has a chi-squared per degree of freedom of $\chi^2_{\rm dof} = 1.20$ which, although larger than the value for LCDM ($\chi^2_{\rm dof} = 1.06$ for $\Omega_m = 0.3$, $\chi^2_{\rm dof} = 1.08$ for $\Omega_m = 0.2$), is much smaller than that for SCDM ($\chi^2_{\rm dof} = 1.75$).

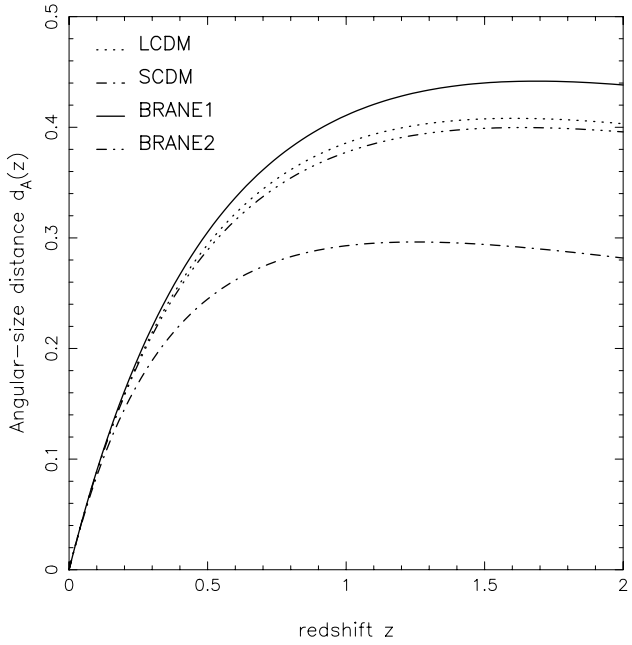

FIG. 9. The angular-size distance (in units of H_0^{-1}) in the braneworld models and in LCDM, SCDM is shown as a function of the redshift. The model parameters are: BRANE1 ($\Omega_m = 0.3, \Omega_l = 0.3, \Omega_{\Lambda_b} = 0$), BRANE2 ($\Omega_m = 0.25, \Omega_l = 0.1, \Omega_{\Lambda_b} = 0$), LCDM ($\Omega_m = 0.3, \Omega_\Lambda = 0.7$). All three models satisfy existing supernovae bounds. Also shown is the standard cold dark matter model (SCDM) with $\Omega_m = 1$.

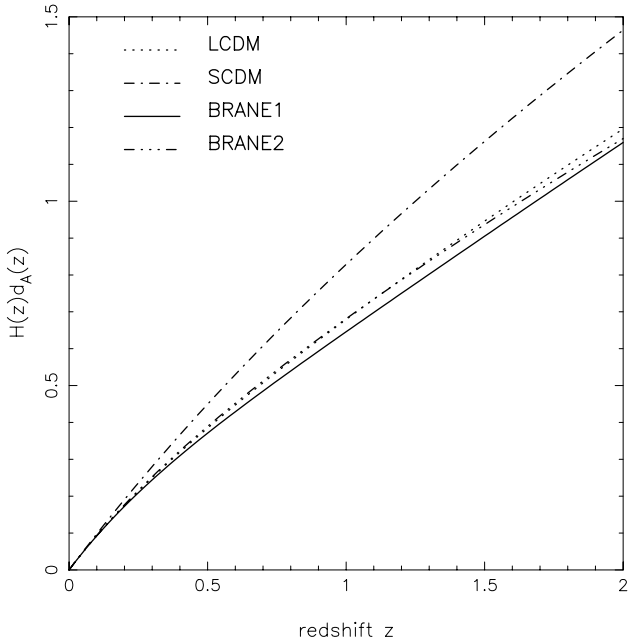

FIG. 10. The dimensionless quantity $H(z)d_A(z)$ which plays an important role in the Alcock-Paczynski test is shown for braneworld models and for LCDM, SCDM as a function of the redshift. The model parameters are the same as in the previous figure.

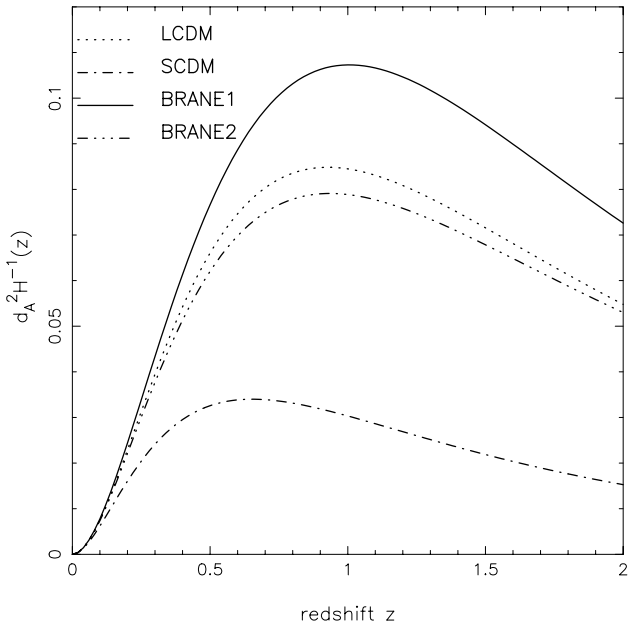

FIG. 11. The quantity $d_A^2 H^{-1}(z)$ which plays a key role in the volume-redshift test is shown for braneworld models and for LCDM, SCDM as a function of the redshift. The model parameters are the same as in the previous figures.

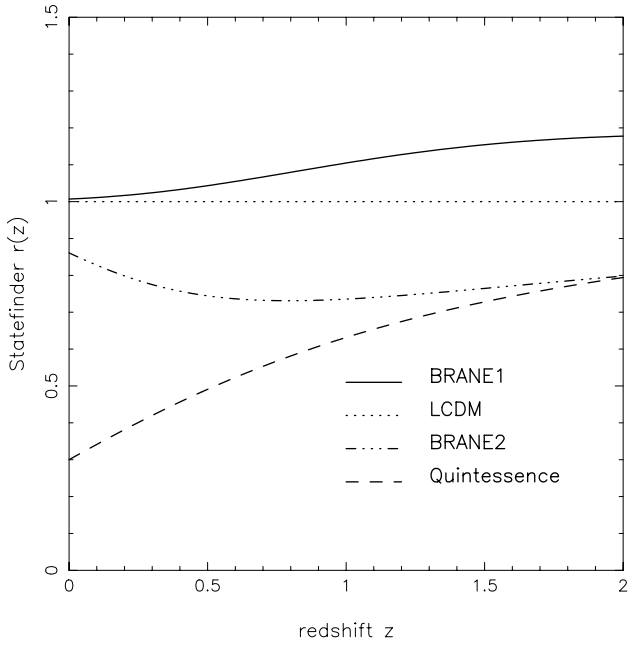

FIG. 12. The dimensionless statefinder $r = \dddot{a}\ /aH^3$ is shown for braneworld models and for LCDM. Also shown is the quintessence model with equation of state $w = -2/3$. The model parameters are the same as in the previous figure.

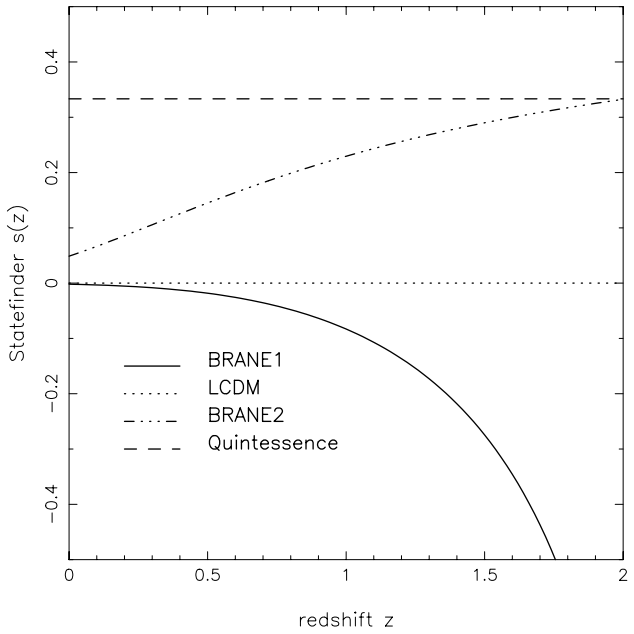

FIG. 13. The dimensionless statefinder $s = (r-1)/3(q-1/2)$ is shown for braneworld models and for LCDM. Also shown is the quintessence model with equation of state $w = -2/3$. The model parameters are the same as in the previous figure.

One may try to constrain braneworld models further using some of the cosmological tests outlined earlier in this paper. Through these tests it may be possible to distinguish between different braneworld models which agree well with current SNe data. To illustrate this we choose two complementary braneworld models: (a) BRANE1 with $\Omega_m = 0.3, \Omega_l = 0.3, \Omega_{\Lambda_b} = 0$, and (b) BRANE2 with $\Omega_m = 0.25, \Omega_l = 0.1, \Omega_{\Lambda_b} = 0$, which satisfy both the high-z SNe observations (at the 1σ level) and the observational constraints on Ω_m. In figure (9) we show theoretical results for the angular-size distance d_A, which is determined from observations of the angle $\Delta\theta$ subtended by a 'standard ruler' of length ℓ at a redshift z, $\Delta\theta = \ell/d_A(z)$. Another useful quantity is $H(z)d_A(z)$, shown in figure (10), which plays a crucial role in the Alcock-Paczynski anisotropy test. We clearly see that the angular-size distance provides a better test with which braneworld models may be distinguished from each other and from rival models such as LCDM and SCDM. The Alcock-Paczynski test may not serve this purpose, since both B1 & B2 give results which are close to each other and to those for LCDM. The reason for this seeming degeneracy lies in the fact that, for B1 (B2), the Hubble parameter $H(z)$ *decreases* (increases) relative to LCDM while the distance d_A *increases* (decreases). Thus $H(z)$ and d_A show opposing tendencies for the braneworld models, which virtually neutralise each other in the combination $H(z)d_A(z)$. Exactly the opposite effect is achieved by the combination $d_A^2(z)H^{-1}(z)$ which plays a key role in the volume-redshift test [19]. In this case the difference between B1 and B2 becomes more pronounced as demonstrated in figure 11. We therefore conclude that the volume-redshift test is probably a better means for differentiating between the two braneworld models B1 & B2 than the Alcock-Paczynski test.

Interestingly the statefinder statistic (18) may also provide us with a useful means by which to discriminate between rival braneworld models and LCDM/quintessence, as demonstrated in figures (12) & (13). Other cosmological tests which are likely to be useful in testing braneworld models include gravitational lensing [24] and the cosmic microwave background [25]. We shall return to these important issues in a future work.

IV. DISCUSSION AND CONCLUSIONS

This paper examines braneworld models of dark energy in the light of recent supernova observations which indicate that the universe is accelerating. The braneworld models which we examine in this paper have several interesting properties which distinguish them both from the cosmological constant as well as from scalar field based 'tracker' models of dark energy. Like the latter, braneworld models presently accelerate, and possess a longer age than the standard cold dark matter model (SCDM). However in marked contrast to both LCDM and tracker models, the luminosity distance in one class of braneworld models, B1, can be *greater* than the luminosity distance in LCDM (for identical values of Ω_m): $d_L^{\rm dS}(z) \geq d_L^{\rm BRANE1}(z) \geq d_L^{\rm LCDM}(z)$, where $d_L^{\rm dS}(z)$ refers to the luminosity distance in spatially flat de Sitter space. In terms of the effective equation of state w, this is equivalent to the assertion that $w \leq -1$. This result is particularly surprising since matter in the braneworld model never violates the weak energy condition $\rho + p \geq 0$. A maximum likelihood analysis which compares braneworld model predictions with high redshift type Ia supernovae data, shows that B1 models provide good agreement with observations if $\Omega_m \gtrsim 0.3$. These results broadly support the analysis of [23] in which 'phantom' dark energy models, having the property $w = P/\rho \leq -1$, were compared against supernova observations. (It should be pointed out, however, that 'phantom models' invariably run into a physical singularity in the future when $\rho_{\rm phantom} \to \infty$, such singularities are absent in the B1 model which remains well behaved at all future times.)

The second braneworld model we consider (B2) has properties which complement those of B1, since $d_L^{\rm LCDM}(z) \geq d_L^{\rm BRANE2}(z) \geq d_L^{\rm SCDM}(z)$. This is equivalent to the assertion that $-1 \leq w \leq 0$. Results of a maximum likelihood analysis show that B2 models are in excellent agreement with SNe data for smaller values of the density parameter $\Omega_m \lesssim 0.25$.

Finally braneworld models also permit the dark energy to be a transient phenomenon. In models of this kind (called disappearing dark energy: DDE) the acceleration of the universe takes place during a transient regime separating past and future matter dominated epochs.

In these braneworld models, the universe does not possess an event horizon and so it may be possible to reconcile a universe which currently accelerates with the demands of string/M-theory. Comparison with Sne bounds shows that the Disappearing Dark Energy models marginally satisfy existing supernova data provided Ω_m is sufficiently small: $\Omega_m \lesssim 0.23$. For larger values of Ω_m, this class of models may be on the verge of being ruled out.

ACKNOWLEDGMENTS

We acknowledge useful discussions with Somak Raychaudhury, Tarun Deep Saini, Yuri Shtanov, Tarun Souradeep and R.G. Vishwakarma. UA was supported for this work by the CSIR.

REFERENCES

[1] Appelquist, T., Chodos, A. and Freund, P.G.O. editors: *Modern Kaluza-Klein Theories*, Addison-Wesley Publishing Co. (1987)

[2] Horava, P. and Witten, E. Nucl. Phys. **B 460**, 606 (1996); Nucl. Phys. **B 475**, 94 (1996).

[3] L. Randall and R. Sundrum, Phys. Rev. Lett. **83**, 3370 (1999) [hep-ph/9905221]; Phys. Rev. Lett. **83**, 4690 (1999) [hep-th/9906064].

[4] P. Binétruy, C. Deffayet, and D. Langlois, Nucl. Phys. B **565**, 269 (2000) [hep-th/9905012]; C. Csáki, M. Graesser, C. Kolda, and J. Terning, Phys. Lett. B **462**, 34 (1999) [hep-ph/9906513]; J. M. Cline, C. Grojean, and G. Servant, Phys. Rev. Lett. **83**, 4245 (1999) [hep-ph/9906523]; P. Binétruy, C. Deffayet, U. Ellwanger, and D. Langlois, Phys. Lett. B **477**, 285 (2000) [hep-th/9910219]. T. Shiromizu, K. Maeda, and M. Sasaki, Phys. Rev. D **62**, 024012 (2001) [hep-th/9910076]. R. Maartens, D. Wands, B. A. Bassett, and I. P. C. Heard, Phys. Rev. D **62**, 041301 (2000) [hep-ph/9912464]; E. J. Copeland, A. R. Liddle and J. E. Lidsey, Phys. Rev. D **64** 023509 (2001) [astro-ph/0006421]; V. Sahni, M. Sami, and T. Souradeep, Phys. Rev. D **65** 023518 (2002) [gr-qc/0105121].

[5] R. Maartens, V. Sahni and T. D. Saini, Phys. Rev. D **63** 063509 (2001) [gr-qc/0011105]; A. Campos and C. F. Sopuerta, Phys. Rev. D **63**, 104012 (2001) [hep-th/0101060]; A. V. Toporensky, Class. Quant. Grav. **18**, 2311 (2001) [gr-qc/0103093].

[6] G. Dvali, G. Gabadadze, and M. Porrati, Phys. Lett. B **485**, 208 (2000) [hep-th/0005016]; G. Dvali and G. Gabadadze, Phys. Rev. D **63**, 065007 (2001) [hep-th/0008054].

[7] V. Sahni and Yu. V. Shtanov, *Braneworlds models of dark energy*, astro-ph/0202346.

[8] A. Riess *et al.*, Astron. J. **116**, 1009 (1998) [astro-ph/9805201];

[9] S. J. Perlmutter *et al.*, Astrophys. J. **517**, 565 (1999) [astro-ph/9812133].

[10] V. Sahni and A. A. Starobinsky, Int. J. Mod. Phys. D **9**, 373 (2000) [astro-ph/9904398].

[11] V. Sahni, Class. Quant. Grav. **19**, 3435 (2002) [astro-ph/0202076].

[12] Yu. V. Shtanov and V. Sahni, Class. Quant. Grav. **19**, L101 (2002) [gr-qc/0204040].

[13] W. Fischler, A. Kashani-Poor, R. McNees, and S. Paban, JHEP **0107**, 3 (2001) [hep-th/0104181]; J. Ellis, N. E. Mavromatos, and D. V. Nanopoulos, *String theory and an accelerating universe*, hep-th/0105206; J. M. Cline, JHEP **0108**, 35 (2001) [hep-ph/0105251]; X.-G. He, *Accelerating universe and event horizon*, astro-ph/0105005.

[14] H. Collins and B. Holdom, Phys. Rev. D **62**, 105009 (2000) [hep-ph/0003173].

[15] Yu. V. Shtanov, *On brane-world cosmology*, hep-th/0005193.

[16] C. Deffayet, G. Dvali, and G. Gabadadze, Phys. Rev. D **65**, 044023 (2002) [astro-ph/0105068]; C. Deffayet, S. J. Landau, J. Raux, M. Zaldarriaga, and P. Astier, Phys. Rev. D **66**, 024019 (2002). [astro-ph/0201164].

[17] V. Sahni, T. Saini, A. A. Starobinsky and U. Alam, *Statefinder – a new geometrical diagnostic of dark energy*, astro-ph/0201498.

[18] C. Alcock and B. Paczynski, Nature **281**, 358 (1979). J. Kujat, A.M. Linn, R.J. Scherrer and D.H. Weinberg, ApJ **S72**, 1 (2001) astro-ph/0112221.

[19] J.A. Newman and M. Davis, ApJ **534**, L11 (2000); astro-ph/0109131.

[20] J. A. Peacock *et al.*, Nature **410**, 169 (2001). J. A. Peacock *et al.*, *Studying large-scale structure with the 2dF Galaxy Redshift Survey*, astro-ph/0204239 . To appear in "A New Era in Cosmology" (ASP Conference Proceedings), eds T. Shanks and N. Metcalfe.

[21] S. Borgani *et al.*, *Measuring Ω_M with the ROSAT deep cluster survey*, astro-ph/0106428.

[22] J. Primack, *Status of Cold Dark Matter Cosmology*, astro-ph/0205391. To appear in the Proceedings of 5th International UCLA Symposium on Sources and Detection of Dark Matter, Marina del Rey, February 2002, ed. D. Cline.

[23] R. R. Caldwell, *A phantom menace?*, astro-ph/9908168.

[24] D. Jain, A. Dev and J.S. Alcaniz, *Brane World Cosmologies and Statistical Properties of Gravitational Lenses*, astro-ph/0206224.

[25] P.S. Corasanti and E.J. Copeland, Phys. Rev. D **65**, 043004 (2002) [astro-ph/0107378]; R. Bean and A. Melchiorri, Phys. Rev. D **65**, 041302 (2002) [astro-ph/0110472].